Acoustic-wave localization in the presence of shear resonances

Ian S. Graham, Luc Piché, and Daniel Levesque
National Research Council, Industrial Materials Research Institute, 75 De Mortagne Boulevard, Boucherville, Québec, Canada J4B 6Y4

Martin Grant
Department of Physics, McGill University, Rutherford Building, 3600 University Street, Montréal, Québec, Canada H3A 2T8
(Received 26 December 1990)

We study, via both experiment and theory, localization of longitudinal-acoustic waves scattered from sites supporting transverse (shear) modes. The experimental system consists of a polymer melt solidifying by the growth of spherical semicrystalline nuclei. We excite this system with acoustic plane waves and measure the transmitted signal. For sufficiently high excitation frequencies we find renormalization of the sound speed and intense absorption peaks over a very narrow range of wave number. These data can be consistently interpreted as signs of localization within the sample. Standard theory, however does not predict localization in this system, since the longitudinal velocity in the scatterers is faster than that in the liquid. However, the solid scatterers support shear modes, which can significantly modify their scattering characteristics. We extend the theory of localization to allow for scatterers supporting shear. This model predicts shear-induced localization in the system we have studied.

I. INTRODUCTION

Consider a medium containing randomly distributed scattering sites, such that the system is characterized by an elastic scattering mean free path l_E. Assume that the inelastic scattering mean free path $l_I \gg l_E$, so that dissipation can be ignored, and that λ, the wavelength of the radiation (or the particle DeBroglie wavelength) satisfies $\lambda \ll l_E$, so that coherent multiple scattering is unimportant. In this case if the system size $L \gg l_E$ then energy is transported diffusively and the transport properties of system are characterized by a diffusion constant D.[1]

Now suppose that the wavelength and elastic scattering MFP satisfy $l_E \approx \lambda$; this is known as the Ioffe-Regel condition.[2] In this case coherent multiple-scattering events cannot be ignored, and in fact can dominate the transport process. This was first noted by Anderson,[3] who showed that this regime should admit a 'localized' state, where transport stops and the wave (in his case the electron wave function) is localized to a finite region in space. This results from long-range coherent multiple-scattering events which dominate transport behavior and which renormalize the diffusion constant to zero.

Localization effects were first investigated in the context of electron transport problems. Several reviews on this subject have recently been published.[4,5] However, since it is a coherent-scattering phenomena, localization should also occur in classical wave scattering. Theoretical work on the classical wave problem shows that all random one- and two-dimensional systems must be localized, and that in three dimensions there can be transitions from unlocalized to localized states. By analogy with the electron transport problem, the boundary between these two states is called a mobility edge. John's replica functional integral approach[6] has provided a succinct proof of this latter point, while several perturbative approaches have allowed for detailed study of the weak-localization regime. These approaches are useful in describing phenomena such as enhanced backscatter[7,8] and speckle.[9-12] Such effects have recently been observed in optical scattering experiments.[9,10,13-16] However, fully localized states have not been observed other than in specially prepared one-dimensional systems.[17,18] This reflects the technical difficulty of fabricating weakly dissipating strongly scattering systems satisfying the Ioffe-Regel condition.

The strongly localized regime has been studied in less detail, since here the perturbative approaches break down. The replica functional integral approach[6,19,20] has proven very successful for analyzing the critical region near the mobility edge. This treatment allowed John to prove the existence of localization transitions in $d=3$ and to predict the critical exponents for the divergence of the absorption as the mobility edge is approached from the conducting side. However, this treatment does not allow explicit calculation of the diffusion constant D or of other physically measurable quantities. Soukoulis and co-workers[21,22] have developed a modification of the coherent-potential approximation, which allows one to predict the position of the mobility edge, but again does not directly yield diffusion constants or velocities. Sheng and Zhang[23] have developed a diagrammatic method which, although only valid at low scattering densities, does yield expressions for these quantities. This is also the case for the self-consistent theory of Condat and Kirkpatrick[24-26] (CK). This latter approach is briefly reviewed below.

In this paper we report evidence of localization phe-

nomena for acoustic waves in a three-dimensional system. Our novel system consists of a polymer melt containing a constant number of spherical, equal-sized nuclei. During the experiment the radius, a, of these nuclei increases with time as the solid semicrystalline phase grows from the liquid. We excite the system by applying an ultrasonic pulse of fixed width and constant frequency. We then measure the attenuation and sound velocity through the sample, as well as the shape of the transmitted sound pulses. By performing these experiments as a function of time we are able to ultrasonically probe the system with a tunable reduced wave number, $\eta \equiv ka$, k being the wave number of the incident sound wave in the liquid phase. For sufficiently high excitation frequencies we observe intense peaks in the attenuation. These peaks are narrow, spanning a limited range of scattering site radii. We also observe renormalization of the wave velocity within the peaks, as well as anomalous forward scattering of the coherent signal. As we discuss below these observations can be consistently interpreted as signs of localization of the acoustic wave within the sample.

These results are somewhat unexpected, as the standard analysis[21–25] does not predict localization under the conditions we consider: here, the longitudinal sound velocity of the scatterers is *faster* than that of the medium. However, our solid scatterers can also support shear waves, which can significantly affect their scattering properties. We have examined the importance of shear by generalizing the work of Condat and Kirkpatrick (CK). In their analysis CK considered scatterers which supported only longitudinal waves, but at a different velocity from the background. We have extended their self-consistent approach to allow for scatterers supporting shear. This additional degree of freedom gives rise to internal resonances within the scatterer and to enhancement of the single-site scattering cross section. This turns out to be sufficient to lower the elastic scattering mean free path to the point where localized states become possible.

The outline of the paper is as follows.[27] In the next section we discuss the experimental method and present the experimental results. These results indicate localization-related phenomena, but in a regime not expected by the standard shear-free analysis. This is followed by a brief review of the theory of classical wave localization, with particular emphasis on the approach of CK. Here we also develop the modifications to the CK theory which are needed to allow scatterers supporting shear, and compare the results of this new theory with the original CK approach in order to illustrate how shear can lead to localization. Finally we use our new theory to examine the role that shear can play in our experimental system. We find that the theory predicts localization in the system we have studied, once shear is taken into account.

II. EXPERIMENT

The details of the experimental apparatus will be presented elsewhere.[28] The sample, a thin 0.5 cm disk, 4.0 cm in diameter, is confined between two vertically-aligned buffer rods having ultrasonic transducers at the outer ends. The buffer rods are free to move vertically to compensate for the thermal expansion of the sample, and the axial length of the assembly can be measured to within ± 1 μm so that sample thickness, and hence volume, can be accurately determined. The whole assembly can be maintained at constant temperatures with a stability of ± 0.1 K. Also, the buffer rods maintain a constant pressure on the sample, so that the experiment is performed under both isothermal and isobaric conditions. For measurements, one of the transducers is energized and provides an effective plane wave across the surface of the sample. Similarly the second transducer, used for detection, is sensitive only to signals coherent across the transducer surface. A homodyne system is used to measure the phase of the transmitted signal with respect to the incident pulse. This allows us to measure both the attenuation and phase velocity through the sample. The data are processed to account for the acoustic properties of the buffer and the buffer-sample acoustic mismatch.[28]

The polymer material used was isotactic polypropylene, (Himont, Varennes, Canada), which has a liquid-solid transition near $T_m = 438$ K. We begin the experiment by annealing the liquid sample at 453 K for 20 min, and then quenching to 425 K. After a delay the solid phase begins to form, via heterogeneous nucleation of solid semicrystalline droplets within the liquid. These droplets appear to nucleate on trace microscopic impurities in the molten polymer, so that n, the number density of nuclei is constant from experiment to experiment.

In a separate experiment we used a transmission polarizing microscope to visualize the evolution of the structure during solidification: characteristic photographs of the growing spheres are shown in Fig. 1. We observed that (1) the nucleation centers were randomly distributed; (2) the growth was radial such that the volume of the individual spherulite is $\Omega = 4\pi a^3/3$; (3) the growth was initiated simultaneously for the different spherulites and therefore their number was constant; and (4) the growth rate was constant for all sites (≈ 1.5 μm/min.) such that the spherulites were of uniform size. The system is consequently highly monodisperse. The spheres continue to grow until contact. Finally the interstitial regions solidify, and the solid phase is fully formed.

The spherulites come into contact at a radius $a(\mathrm{RCP}) = 125$ μm, which corresponds to a random-close-packed (RCP) structure for the packed spheres in the solid phase. Under this assumption we can determine the time-independent number density of spherulites $n \approx 8 \times 10^4$ cm^{-3}. We also measure the densities of the pure fluid, $\rho = 0.82$ gm cm^{-3} and pure solid, $\rho_s = 0.89$ gm cm^{-3}. Therefore, using n and the measured (time-varying) total volume of the polymer sample we can determine the radii of the scatterers as a function of time, as the solid phase is formed. The total time between the onset of nucleation and the formation of random-close-packed spheres takes on the order of seven to eight hours.

We probed the system with ultrasonic longitudinal-wave pulses of duration ≈ 6 μsec, with a rise time and fall time of ≈ 2 μ sec. Therefore the system does not evolve on the time scale of the acoustic measurements. We mea-

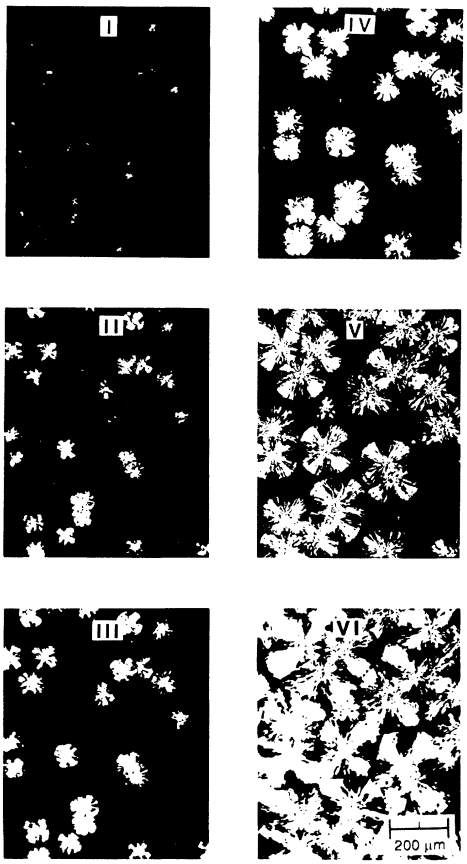

FIG. 1. Photomicrographs showing the evolution with time of the solid phase spherulites.

sured the attenuation and sound velocity of the *coherent* part of the transmitted signal. As mentioned above we excite the sample with a spatially coherent signal, and detect only the spatially coherent part of the transmitted pulse. This should be contrasted with typical optical experiments, where the detectors are not sensitive to spatial coherence. We excited the samples at frequencies of 1.75, 2.5, 4.88, 6.0, and 8.0 MHz, in order to probe the system on different length scales, and also to allow separation of single-scatterer from multiple-scatterer (or other) phenomena.

Figure 2(a) shows the evolution of specific volume v during solidification under isothermal ($T=410$ K) and isobaric ($p=200$ kPa) conditions, close to those of the photomicrographs in Fig. 1. In Fig. 2(b) we illustrate the concommittant changes in the velocity c and attenuation a for 2.5 MHz longitudinal waves. As mentioned above the results for the specific volume provide a direct measurement for the volume content of the semicrystalline spherulites. Here RCP occurs near the 1 hour mark.

At short times the velocity describes a shallow dip, indicating that the density initially increases more rapidly than the effective modulus. Thereafter, c increases steadily until the spheres start to percolate and come into contact, whereupon it gradually levels off at a value corresponding to the solid phase. In parallel the attenuation initially remains close to the value $a_I \approx 4$ dB cm^{-1} ($l_I \approx 2.5$ cm) associated with the viscosity of the melt. Later the attenuation increases rapidly due to elastic scattering from the solid spheres, reaching a value

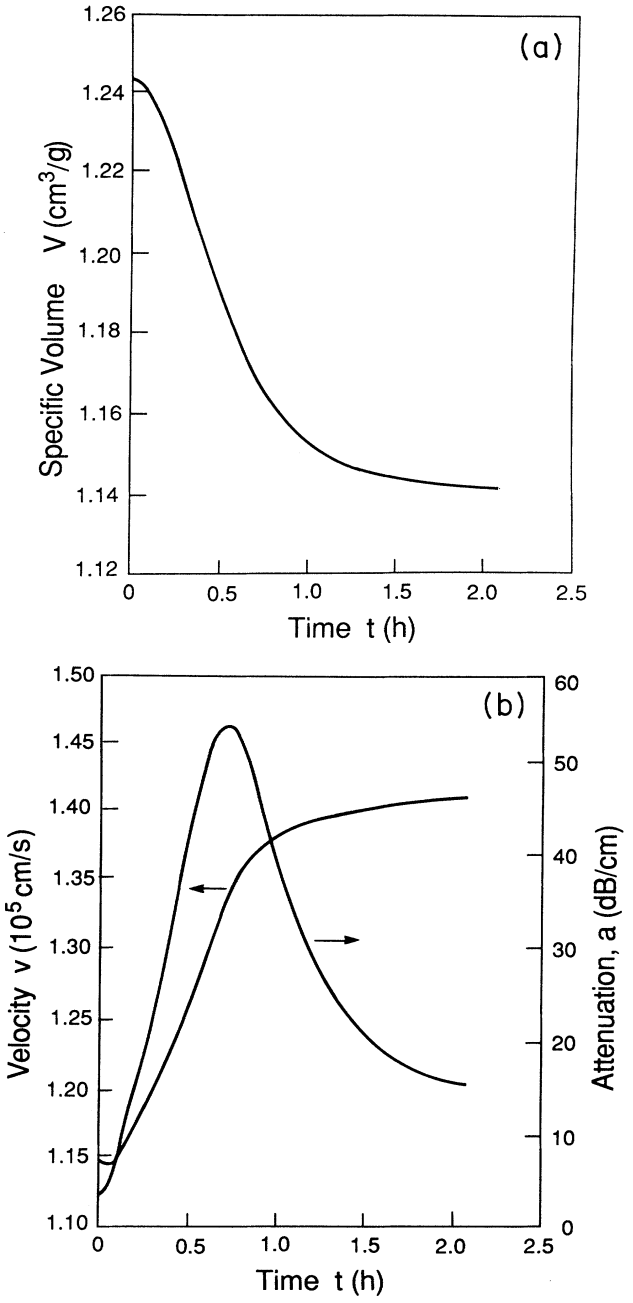

FIG. 2. Data showing the variation of (a) the specific volume v and (b) the phase velocity c and attenuation l^{-1} of 2.5 MHz acoustic waves as a function of time t. In this example solidification occurs rapidly because the sample was constrained under low pressure (200 kPa). The remaining data were obtained under a pressure of 2000 kPa. This higher pressure was used to increase the degree of undercooling and to slow the solidification process.

$a_E \approx 18$ dB cm^{-1} at around the 15-min mark. This corresponds to an elastic mean free path $l_E \approx 0.5$ cm, and marks the crossover into the diffusive regime. The attenuation continues to increase until the percolation threshold, whereupon it decreases as the medium becomes more homogeneous. Here the data implies $\lambda/l_E \approx 0.3$ near the maximum in the attenuation. We find that even when crystallization is complete, the structure is not sufficiently rigid to support shear waves over a distance much larger than the wavelength λ. The value for the shear wave velocity, in this and other cases, was estimated by extrapolating low-temperature data.

The actual measurements presented in the following were performed at a higher pressure of 2000 kPa, in order to provide greater undercooling. This slows the solidification process and allows for greater resolution in the experiment.

In Fig. 3 we plot our experimental results for the acoustic attenuation, l^{-1}, as a function of dimensionless wave number η, where $\eta \equiv 2\pi\nu a/c$, ν being the excitation frequency, a is the radius of the nuclei, and where c, the velocity of sound in the liquid, is 1250 m/sec. Here the different curves are truncated at values of η coinciding with random close packing. Also, we have subtracted off the residual attenuation associated with the viscosity of the liquid phase, ≈ 0.5 cm^{-1}. For the semicrystalline solid, the inelastic absorption is larger, ≈ 2 cm^{-1}. However l_I for both liquid and solid phases is still long on the scale of interparticle spacings.

At excitation frequencies of 2.5 MHz and lower, we observe a slow rise and subsequent fall in attenuation of the signal as the solid phase nucleates. However, at 4.88, 6.0, and 8.0 MHz we find distinct narrow absorption peaks. The peaks lie at different values of η for these different excitation frequencies. They are therefore not due to single-site resonances, since such peaks must lie at the same dimensionless wave number η, regardless of frequency. Coincident with these peaks we observe sudden changes in the measured renormalized sound velocity, $\bar{c}$, as illustrated in Fig. 4(a). This is further evidence of a resonance phenomenon.

The shape of the transmitted pulses also helps in characterizing the attenuation. Figure 4(b) shows shapes typical of the transmitted pulse envelopes, taken at various positions marked in the absorption peak in Fig. 4(a). Far from the strong absorption regions, the transmitted pulse is simply a diminished version of the excitation pulse, with similar shape and length. However, near the absorption region the transmitted pulse becomes significantly lengthened, and in fact splits into two pulses: one that is directly transmitted and one that is delayed. The delayed pulse is not due to reverberations within the sample, as it occurs too soon after the initial pulse. In any case, the attenuation is so high that any true reverberated signal would have negligible amplitude and would not be detected. The position of the delayed pulse is also largely independent of the excitation pulse length.

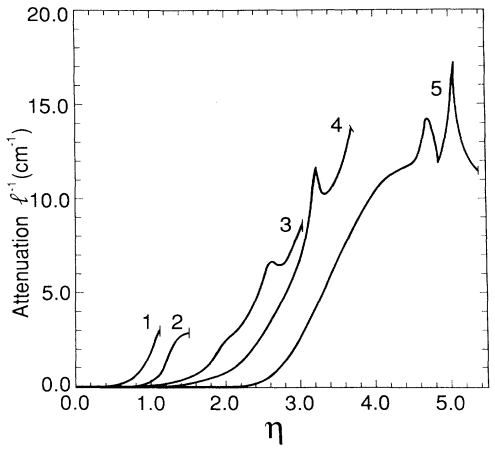

FIG. 3. Experimental results for attenuation l^{-1} as a function of reduced wave number η for acoustic waves of frequencies 1.75, 2.5, 4.88, 6.0, and 8.0 MHz. The curves have been truncated at the volume fraction for random close packing of the spheres with radii a(RCP) = 125 μm.

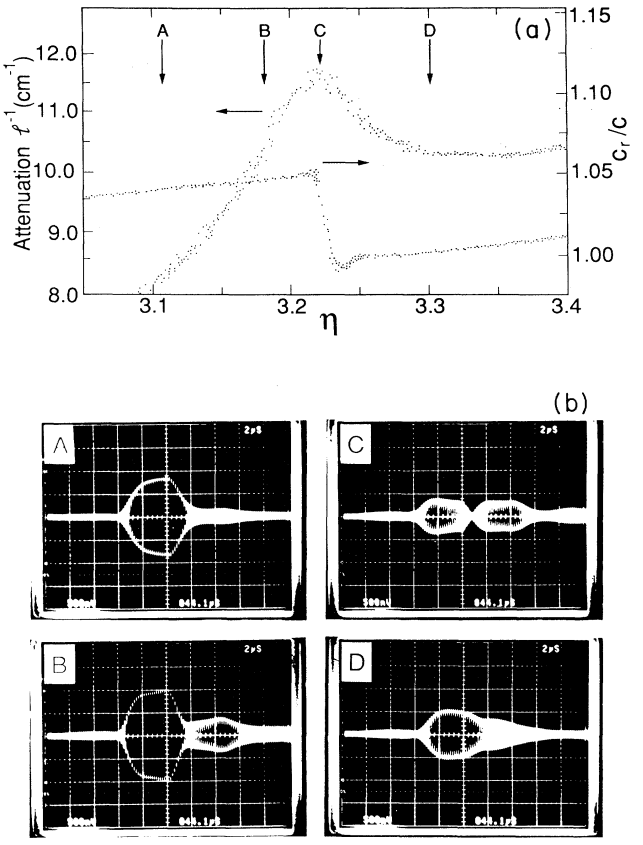

FIG. 4. (a) Attenuation, l^{-1}, and the ratio of the measured velocity to the velocity in the liquid $\bar{c}/c$ as a function of reduced wave number η, in the vicinity of the absorption peak for the 6.0 MHz data. (b) Oscilloscope photographs showing the shape of the transmitted signals; the labels A, B, C, and D refer to values of η indicated by the corresponding labels in (a). Relative to signal A the amplifier gain is up by 12 dB for signal B, 14 dB for signal C and 10 dB for signal D.

Thus lengthening the incident pulse merely turns the delayed pulse into a "bump" on the tail of the main transmitted pulse. Several possible sources of this pulse can be ruled out. First it cannot arise from reradiation from excited, oscillating spheres, as such a signal would be incoherent and hence undetectable by our system. We have also ruled out saturation of a resonant absorption mechanism by verifying that the effect remains after varying the input signal amplitude by ± 10 dB. Finally we note that the first absorption peak occurs below the percolation threshold for the solid phase, so that bulk resonances of the entire system are unlikely to play a role.

Having ruled out these alternative possibilities we interpret the delayed pulse as a resonant forward-scattering mechanism, in which the transmitted pulse is followed by an echo arising from time-reversed scattering paths in the same direction as the incident wave. This is analogous to the resonant back scattering seen in optical experiments on localization. In this way we can consistently interpret our results of anomalous attenuation at nonconstant η, sound renormalization and anomalous forward scattering as signs of localization of sound within the sample.

III. THEORY

Our starting point is the scalar wave equation in a nondispersive medium:

$$\left[\nabla^2-\frac{1}{c^2}\frac{\partial^2}{\partial t^2}\right]\phi(x,t)=0 , \tag{1}$$

where c, here a real number, is the longitudinal wave velocity and ϕ is the local displacement field. The solution of this equation in the presence of scatterers is difficult and requires suitable approximation techniques. This takes great care, as the method must treat the scatterers in a realistic way and must also ensure that the process of "averaging" over the disorder does not throw away correlated multiple-scattering events.

Such scattering problems are best treated via the Green's-function scattering formalism, so the problem becomes one of finding ways to calculate ensemble averages of the one-particle $\langle G_\omega^+(\mathbf{k},\mathbf{k}')\rangle$ and the two-particle $\langle |G_\omega^+(\mathbf{k},\mathbf{k}')|^2\rangle$ Green's function (GF). The former provides information about renormalization of the velocity due to scattering. The latter corresponds to the propagator for the wave energy density, from which one can derive a frequency-dependent diffusion constant $D(\omega)$ for energy propagation. When coherent-scattering effects are unimportant this gives rise to the equations of radiative transport theory.[6] However, when coherent multiple scattering is important the diffusion constant can be rescaled to zero. This is the signal for localized states, so that an expression for $D(\omega)$ is the goal of the analysis. We shall pursue this goal using the self-consistent approach of Condat and Kirkpatrick (CK). This has the advantage of being straightforwardly extensible to the types of systems we wish to study—a background medium propagating only longitudinal pressure waves containing spherical scatterers supporting both shear and longitudinal waves.

Consider a medium density ρ which propagates longitudinal waves with a frequency-independent velocity c. This medium contains a number of identical spherical scatterers of radius a. We denote the number density of scatterers by n, so that the volume fraction of scatterers is $n^*=4\pi a^3 n/3$. The fraction n^* must be small so that a perturbative expansion around the pure fluid is possible.

The CK theory[24,25] can be summarized as follows. Using diagrammatic techniques they calculate perturbative approximations for the averaged one- and two-particle Green's functions in terms of the single-site scattering matrix $T(\mathbf{k},\mathbf{k};\omega)$. The single-particle GF is solved using Dyson's equation, under the approximation that n^* is small. This gives rise to a modified wave velocity, $\bar{c}$, renormalized due to scattering.

The two-particle GF is determined by solving the Bethe-Salpeter equation via diagrammatic summation approximations to derive an expression for a "Boltzmann" diffusion constant, $D_B(\omega)$. This represents the diffusion constant arising purely from incoherent scattering processes. CK then develop a self-consistent theory for the true diffusion constant $D(\omega)$ due to both coherent- and incoherent-scattering processes. This involves summing a family of diagrams which are expected to be important for localization (maximally crossed diagrams) and taking a self-consistent approximation to the resulting divergent expression for $D(\omega)$. This gives an analytic expression for the diffusion constant in terms of the single-site scattering matrix T and the renormalized velocity $\bar{c}$. The results of the model then depend on the parameters n^* and c and on the scattering matrix T.

We now briefly review the theoretical framework of CK. The unperturbed GF for the wave equation (1) is, in momentum-frequency space

$$\begin{aligned} G_{0,\omega}^{\pm}(\mathbf{k},\mathbf{k}') &= \delta(\mathbf{k}-\mathbf{k}')G_{0,\omega}^{\pm}(k) \\ &= \frac{\delta(\mathbf{k}-\mathbf{k}')}{(\omega\pm i\epsilon)^2-c^2k^2} , \end{aligned} \tag{2}$$

where the $+$ ($-$) superscript refers to the retarded (advanced) form. Given a single scatterer at position x the single-particle GF can be written in terms of the unperturbed GF as[26,25]

$$\begin{aligned} G_\omega^+(\mathbf{k},\mathbf{k}') &= G_{0,\omega}^+(\mathbf{k},\mathbf{k}') \\ &\quad + e^{i\mathbf{x}\cdot(\mathbf{k}'-\mathbf{k})}G_{0,\omega}^+(k)T(\mathbf{k},\mathbf{k};\omega)G_{0,\omega}^+(k) . \end{aligned} \tag{3}$$

If we now average over random configurations of the scatterers, assuming the system to be homogeneous, $\langle G_\omega^+(\mathbf{k},\mathbf{k}')\rangle$ is diagonal and Dyson's equation allows expression of the averaged Green's function in terms of the self-energy $\Sigma_k(\omega)$;

$$\langle G_\omega^+(\mathbf{k},\mathbf{k}')\rangle=\delta(\mathbf{k}-\mathbf{k}')\frac{1}{G_{0,\omega}^+(k)^{-1}-\Sigma_k(\omega)} . \tag{4}$$

The self-energy can now be expanded in terms of n^*, which to lowest order gives[25]

$$\Sigma_k(\omega)=\frac{6n^*\pi^2}{a^3}T(\mathbf{k},\mathbf{k};\omega)$$
$$=\gamma_k(\omega)-i\beta_k(\omega)\ . \tag{5}$$

Thus the self-energy depends only on the single-scatterer T matrix. The imaginary part corresponds to attenuation of a coherent wave due to scattering. Of particular interest is the real part which, upon inspection of Eqs. (5) and (2), is seen to give rise to a frequency-dependent renormalized speed of sound;

$$\frac{1}{\tilde{c}(\omega)^2}=\frac{1}{c^2}\left[1-\frac{\gamma_{\omega/c}(\omega)}{\omega^2}\right]\ . \tag{6}$$

The solution for the two-particle GF is more problematic. CK show that the Fourier-Laplace transform of the two-particle GF, averaged over the disorder, is proportional to a diffusive hydrodynamic pole:

$$\langle|G_{\epsilon,k}(\omega)|^2\rangle\sim\frac{1}{-i\epsilon+D(\omega,\epsilon)k^2}\ , \tag{7}$$

where ϵ is the external frequency. Localization occurs when $\lim_{\epsilon\to 0}D(\omega,\epsilon)\to-i\epsilon\zeta^2(\omega)+O(\epsilon^2)$. This implies that the spatial energy density does not decay with time and is localized within a spatial region of size $\zeta(\omega)$.

To find an expression for D, CK considered only incoherent-scattering processes and assumed n^* to be small. Then the Bethe-Salpeter equation can be solved to derive the following form for the "Boltzmann" diffusion constant

$$D_B(\omega)=-\frac{c^5}{9n\pi^3}\left[\int d\hat{\mathbf{p}}\hat{\mathbf{p}}_x\int d\hat{\mathbf{k}}\left|T_{\hat{\mathbf{p}}\,\hat{\mathbf{k}}}\left[\frac{\omega}{c}\right]\right|^2\times(\hat{\mathbf{k}}_x-\hat{\mathbf{p}}_x)\right]^{-1}\ , \tag{8}$$

where

$$T_{\hat{\mathbf{p}}\,\hat{\mathbf{k}}}\left[\frac{\omega}{c}\right]=T\left[\mathbf{p},\mathbf{k};\frac{\omega}{c}\right]\Bigg|_{p=k=\omega/c}\ , \tag{9}$$

and where the $\hat{\mathbf{k}}$, etc. refer to unit vectors. This depends on the details of the scattering solely through the single-site T matrix. This diffusion constant, which would describe the behavior of the system in the absence of coherent scattering, can be used to define a transport mean free path,

$$l_T(\omega)=\frac{3}{c}D_B(\omega)\ . \tag{10}$$

This quantity is later important as an integral cutoff.

Coherent-scattering effects are taken into account by including the maximally crossed diagrams within the perturbative expansion, since these are expected to be dominant coherent terms. This is insufficient to describe strong localization, however, as it is only a perturbative approach. CK extended this to develop a self-consistent theory for the diffusion constant. This yields the following form for D in the limit $\epsilon\to 0$

$$D(\omega,\epsilon)=D_B(\omega)+\frac{3\tilde{c}\beta_{\omega/c}(\omega)D_B(\omega)}{4\pi^2\omega^3}\times\int_0^Q\frac{d\mathbf{q}'}{i\epsilon D^{-1}(\omega,\epsilon)-(q')^2}\ . \tag{11}$$

The wave number cutoff, Q, is somewhat arbitrary. CK assume that $Q\sim l_T^{-1}$, and investigated the behavior for various proportionalities. Following CK we will take $Q=6\pi l_T^{-1}$. However, the results are quite dependent on the value of this cutoff, so we can expect no better than qualitative agreement with experiment.

With $Q=6\pi l_T^{-1}$ one can evaluate Eq. (11) to give

$$D(\omega)=D_B(\omega)\left[1-\frac{6\beta_{\omega/\tilde{c}}(\omega)}{\tilde{c}D_B(\omega)}\left[\frac{\tilde{c}}{\omega}\right]^3\right]\ . \tag{12}$$

The velocities on the right-hand side of Eq. (12) have been renormalized, as required by the self-consistent nature of the theory. Also of interest is the ratio D/D_B, which indicates the importance of coherent backscatter to the total diffusion.

Equations (6), (8), and (12) are the core of the CK localization theory. All we need now is an expression for the scattering matrix, T. In the far-field limit T can be written in terms of the scattering amplitude

$$T_{\hat{\mathbf{p}}\,\hat{\mathbf{k}}}(\omega/c)=-\frac{c^2}{2\pi^2}\Phi^+(\theta)\ . \tag{13}$$

The scattering amplitude $\Phi^+(\theta)$ can be found by solving for the scattering of a plane wave from a single scatterer. The corresponding single-site scattering cross section is also of interest, and is given by

$$\sigma=\frac{4\pi}{k}\,\mathrm{Im}\Phi^+(0) \tag{14}$$

or by the appropriate angular integral of $\Phi^+(\theta)$.

We can now write the renormalized velocity in terms of Φ^+ as

$$\frac{1}{\tilde{c}(\omega)^2}=\frac{1}{c^2}\left[1+\frac{3n^*}{\eta^2}\,\mathrm{Re}\left[\frac{\Phi^+(0)}{a}\right]\right] \tag{15}$$

and using the forward-scattering theorem one also obtains

$$\frac{D}{D_B}=1-\frac{9}{2\pi^2}\frac{\lambda^2}{l_El_T}=1-\frac{81(n^*)^2}{8\tilde{\eta}^2}I_1I_2 \tag{16}$$

where

$$I_1=2\int_0^\pi d\theta\sin\theta\left|\frac{\Phi^+(\theta)}{a}\right|^2=\frac{4a}{3n^*l_E}\ , \tag{17}$$

$$I_2=2\int_0^\pi d\theta\sin\theta(1-\cos\theta)\left|\frac{\Phi^+(\theta)}{a}\right|^2=\frac{4a}{3n^*l_T}\ .$$

With the chosen cutoff Q the condition for localization becomes $\lambda\approx\sqrt{l_El_T}$, which differs somewhat from the Ioffe-Regel condition. One notes, for example, that l_T can be 10 times larger than l_E when the scattering is

highly asymmetric.[29]

CK consider scattering spheres with density ρ_s and which propagate longitudinal waves with a velocity c_s. The relevant parameters then turn out to be $\Delta=\rho/\rho_s$ and $M=c/c_s$, the ratios of the densities and wave velocities. CK showed that the localization behavior should be seen, for experimentally reasonable volume fractions n^*, for large values of M, i.e., $M \gtrsim 1.5$. This corresponds to slow scatterers in a fast medium, for example, gas bubbles in a liquid background. Such systems, however, present significant experimental difficulties such as polydispersity and high absorption. Conversely, given structureless scatterers, localization is unlikely in many systems which have $M<1$, owing to the low single-site scattering cross section for M in this regime.

Consider instead solid spheres in a fluid background. In this case $M<1$, so the above treatment does not predict localization. However, solid spheres can support transverse as well as longitudinal excitations, so that the above analysis is clearly insufficient. Motivated by this fact, we now extend the scattering analysis to treat scatterers supporting shear, and to show how this significantly affects the behavior.

Following standard approaches[30] we define the incident, scattered and internal displacement waves in terms of the two fields ψ and π. These fields correspond, respectively, to the longitudinal and transverse parts of the wave. The incident plane wave in the positive z axis direction is derived from the field ψ^i, which is given by

$$\psi^i=\sum_{m=0}^{\infty} i^m(2m+1)\frac{1}{k}j_m(kr)P_m(\cos\theta) . \tag{18}$$

where P_m are Legendre polynomials and the j_m are spherical Bessel functions. The outgoing scattered field ψ^o can be defined similarly,

$$\psi^o=\sum_{m=0}^{\infty} i^m(2m+1)a A_m h_m(kr)P_m(\cos\theta) , \tag{19}$$

where $h_m=j_m+iy_m$ are spherical Hankel functions of the first kind. Within the scatterers there are both longitudinal modes,

$$\psi^s=\sum_{m=0}^{\infty} i^m(2m+1)aC_m j_m(k_s r)P_m(\cos\theta) , \tag{20}$$

and shear modes,

$$\pi^s=\sum_{m=0}^{\infty} i^m(2m+1)aD_m j_m(\kappa r)P_m(\cos\theta) , \tag{21}$$

where c_s^t is the transverse wave velocity in the scatterers, and $\kappa=\omega/c_s^t$ is the corresponding transverse wave number.

To determine the amplitude of the scattered wave, we solve the boundary conditions at the interface between the scatterer and the fluid. These boundary conditions are those of continuity of the radial displacement

$$s_r^i+s_r^o=s_r^s \tag{22}$$

and continuity of the stresses

$$\sigma_{rr}^i+\sigma_{rr}^o=\sigma_{rr}^s \tag{23}$$

$$\sigma_{\theta r}^s=0 . \tag{24}$$

The displacements and stresses are, in terms of the fields,

$$s_r=-\frac{\partial\psi}{\partial r}-\frac{1}{r}\Omega\pi , \tag{25}$$

$$\sigma_{\theta r}=\rho\omega^2\left\{\psi+\frac{2}{\kappa^2}\left[\frac{2}{r}\frac{\partial\psi}{\partial r}+\frac{1}{r^2}\Omega\psi-\frac{\partial}{\partial r}\left[\frac{1}{r}\Omega\pi\right]\right]\right\} , \tag{26}$$

where Ω is the Legendre operator

$$\frac{1}{\sin\theta}\frac{\partial}{\partial\theta}\left[\sin\theta\frac{\partial}{\partial\theta}\right] . \tag{27}$$

Here ρ, k, and κ are the density, longitudinal wave vector, and transverse wave vector in the appropriate component. Outside the scatter $\kappa\equiv 0$.

It is straightforward to solve these boundary conditions for the amplitude coefficients A_m. The angle distribution function is then given by

$$\Phi^+(\theta)=-i\sum_{m=0}^{\infty}(2m+1)a A_m P_m(\cos\theta) . \tag{28}$$

This depends on three parameters, Δ and M as defined above and a third parameter Q given by

$$Q=c_s^t/c_s . \tag{29}$$

In terms of these parameters the boundary conditions reduce to the following system of linear equations for the coefficients A_m, C_m, and D_m:

$$C_m[(m-1)j_m(k_s a)-k_s a j_{m+1}(k_s a)]=D_m\{[m^2-1-\tfrac{1}{2}(\kappa a)^2]j_m(\kappa a)+\kappa a j_{m+1}(\kappa a)\} , \tag{30}$$

$$\frac{1}{ka}[mj_m(ka)-kaj_{m+1}(ka)]+D_m m(m+1)j_m(\kappa a)=C_m[mj_m(k_s a)-k_s a j_{m+1}(k_s a)]-A_m[mh_m(ka)-kah_{m+1}(ka)] , \tag{31}$$

$$\frac{M^2\Delta}{Q^2}[kaj_m(ka)+(ka)^2 A_m h_m(ka)]=C_m\{[(\kappa a)^2-2m(m-1)]j_m(k_s a)-4k_s a j_{m+1}(k_s a)\}+D_m 2m(m+1)[(m-1)j_m(\kappa a)-\kappa a j_{m+1}(\kappa a)] , \tag{32}$$

where $k_s = \omega/c_s \equiv Mk$ and $\kappa = \omega/c_s^t \equiv Mk/Q$. These equations can be straightforwardly solved to yield the desired coefficients A_m.

We can now examine how transverse modes affect localization behavior. We shall consider the case of a fixed scatterer volume fraction $n^* = 0.18$ and scatterers which propagate longitudinal waves faster than the bulk, viz., $M = 0.5714$ $(1/M = 1.75)$. In the absence of transverse modes this should not allow localization. We have examined the behavior both in the absence $(Q = 0)$ and presence $(Q = 0.5)$ of such transverse modes, calculating the theoretical predictions for the single-site scattering cross section, the importance of coherent scattering to diffusion (D/D_B), the renormalized velocity and the attenuation length. The results are shown in Figs. 5 and 6, plotted against the dimensionless wave number $\eta = ka$, where k is the wave number of the wave in the majority medium and a is the radius of the scattering sites.

The importance of shear resonances is strikingly evident. In the absence of transverse modes the single-site scattering cross section is always small, and the calculated diffusion constant is equivalent to the Boltzmann value, viz., $D/D_B \equiv 1$. Coherent-scattering effects are unimportant and propagation is entirely diffusive.

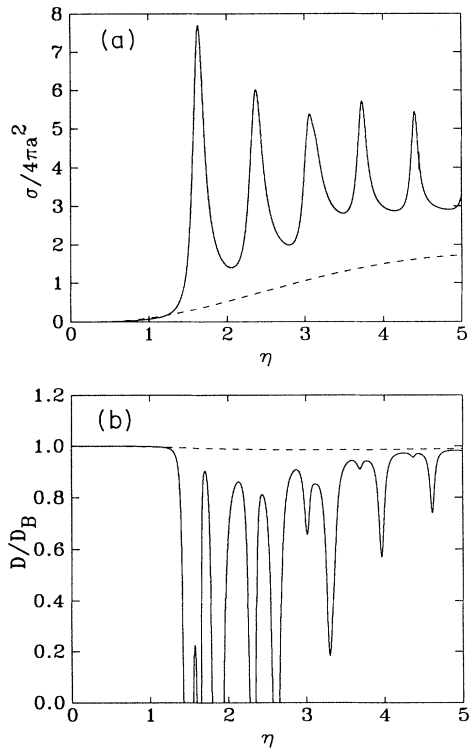

FIG. 5. (a) Single-site scattering cross section $\sigma/4\pi a^2$ and (b) diffusion constant ratio D/D_B as a function of reduced wave number $\eta \equiv ka$, for the case $n^* = 0.18$ and $M = 0.5714$ $(1/M = 1.75)$, $\Delta = 1$. Shown are the results in the absence (dashed line $Q = 0$) and in the presence (solid line $Q = 0.5$) of shear modes within the scatterers.

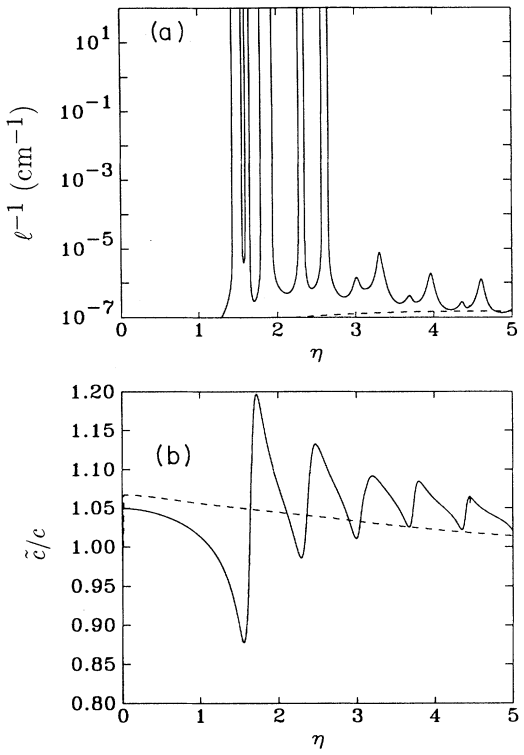

FIG. 6. (a) Attenuation, l^{-1}, and (b) ratio of renormalized velocity to velocity in the liquid, $\tilde{c}/c$, as a function of reduced wave number, η for the two situations presented in Fig. 5. The localization peaks are clearly evident.

When shear is present this situation is completely changed. Coupling between the transverse and longitudinal modes within the scatterers gives rise to strong internal resonances, which are clearly seen in the single-site cross section. These strong resonances allow coherent scattering to become important, so that near the single-site scattering resonances the diffusion constant can be renormalized to zero, as seen in Fig. 5(b). Localization effects due to such internal resonances can therefore occur for moderate scatterer volume fractions.

In an acoustic scattering experiment one can directly measure the attenuation and phase velocity of the transmitted wave. These quantities are shown in Fig. 6, where we plot the attenuation $l^{-1} \equiv c/[3D(\omega)]$ in cm^{-1}, assuming a velocity in the fluid of 2650 m/sec, and the ratio of the renormalized phase velocity to the velocity in the background fluid, $\tilde{c}/c$. The narrow absorption peaks in the attenuation are due to coherent scattering, while the strongest peaks correspond to localized states. Associated with these peaks we note significant renormalization of the sound velocity. However, peaks in this dispersion relation are not necessarily coincident with peaks in the attenuation, as the velocity renormalization is, within this analysis, a single-scatterer calculation while the attenuation calculation takes multiple scattering into account.

IV. DISCUSSION

We now examine what our theory predicts for our acoustic scattering experiment. Theoretical results corresponding to the known values for solid and liquid phase densities and longitudinal wave velocities are shown in Figs. 7 through 8. Here the results have been truncated to show only those data for which $n^* \lesssim 0.4$, since the approximations taken in the development of the theory are unlikely to be valid for larger n^*.

Figure 7 shows the single-site scattering cross-section. The curve shown corresponds to our best estimate for the transverse velocity: the experiment only allows us to determine an upper bound on this quantity, $c_s^t \lesssim 0.3 c_s$ ($c_s^t \lesssim 450$ m/sec). The sharp, shear-induced resonances are clearly evident. We note that this resonance behavior is strongly dependent on Q (not shown) so that decreasing Q by only 10% can significantly affect the position and amplitude of the resonances. This in turn affects the position and magnitude of the coherent scattering resonances shown in Fig. 8.

As mentioned above, even small changes in Q can significantly affect the position and nature of the localized resonances. There is also (not shown) a strong dependence on n, the number density of scatterers, a quantity that is also known only approximately. Therefore we can expect at best qualitative agreement between experiment and theory. We also note that scatterer polydispersity has not been taken into account. Although the system is highly monodisperse, even a small degree of polydispersity leads to broadening of the peaks and to weakening of the narrower resonances.

We now examine theoretical predictions for the attenuation at excitation frequencies of 1.75, 2.5, 4.88, 6.0, and 8.0 MHz, showing characteristic results in Fig. 8. The sharp coherent-scattering-induced absorption peaks are clearly evident. The tallest peaks ($l^{-1} > 10$ cm^{-1}) would correspond, in our system, to fully localized states. Thus our model predicts that localization can occur in the systems we have studied. At high frequencies there is quite reasonable agreement between the peak positions predicted by the theory and those seen in experiment. However, at lower frequencies the theory predicts localization peaks that are not observed experimentally.

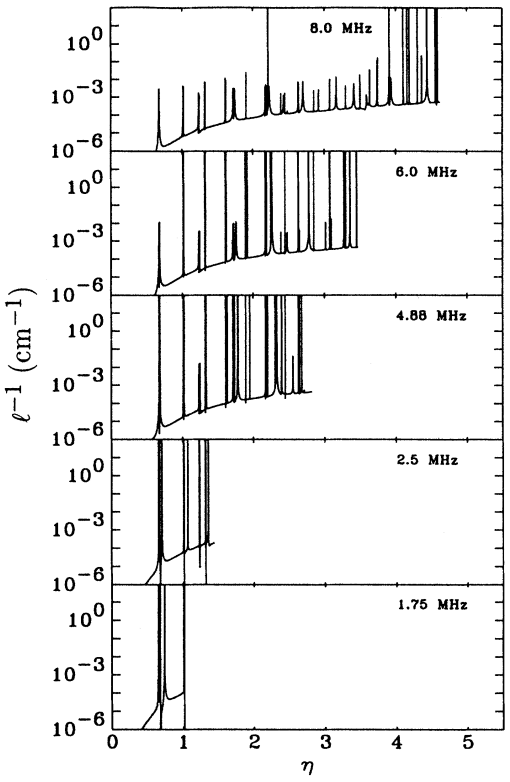

FIG. 8. Attenuation l^{-1} as a function of reduced wave number for acoustic waves of frequencies 1.75, 2.5, 4.88, 6.0, and 8.0 MHz. The parameters are the same as Fig. 6. The curves are truncated above $n^* = 0.4$.

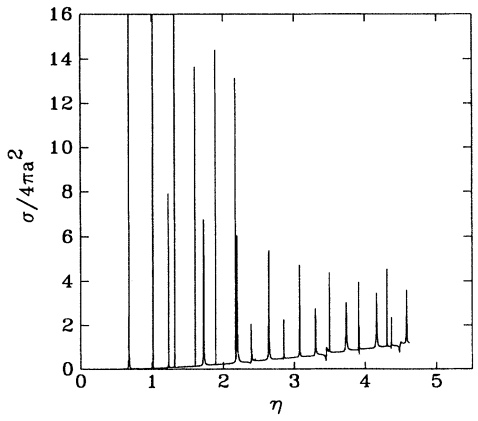

FIG. 7. Single-site scattering cross section as a function of reduced wave number η for $M = 0.477$ and $\Delta = 0.828$ and for $Q = 0.25$. These parameters come from the following values for the densities and velocities in the pure fluid and solid, respectively: $\rho = 0.82$ gm cm^{-3}, $c = 1240$ m sec^{-1}, $\rho_s = 0.99$ gm cm^{-3}, $c_s = 1600$ m sec^{-1}, and $c_s^t = 400$ m sec^{-1}.

The reason for this discrepancy is not clear. One possibility is that smaller-radii scattering spheres are too small to behave in the ideal manner assumed by our analysis. We note that the intense peaks in the high frequency curves correspond to scatter radii on the order of 105 μm, while the intense peaks in the low frequency results correspond to radii on the order of 50 μm, consistent with this argument. To check this point we need a more detailed understanding of the structural properties of the growing solid spheres. Unfortunately such data are not experimentally accessible. We also note that the spheres should be viscously coupled when close on the scale of the acoustic wavelength. This can lead to an enhancement of the coupling between adjacent spheres and hence to an enhancement of the effective scattering cross section. Such effects are not included in our formalism.

At this point we note an alternative explanation for our results, based on recent experimental work by Weitz *et al.*[31] Weitz *et al.* have used Brillouin scattering to ex-

amine the dispersion relation for suspensions of hard-sphere colloids at packing fractions between 15 and 50%. At high packing fractions ($\gtrsim 20\%$) they find that the dispersion curve divides into two branches, one predicting velocities faster than that due to a linear interpolation of the pure fluid and pure solid, the other slower. These modes are interpreted as being due to an acoustic wave propagating through the composite medium (fast) and one propagating along the interface between spheres (slow). This slow mode arises when the exponentially damped shear wave in the fluid can couple to an adjacent sphere, thereby allowing an interfacial wave to propagate through the region between them. Theoretical work[32] has confirmed this analysis for this experimental situation: here the velocity in the fluid is 1.2×10^5 cm/sec while, in our notation, $M=0.44$, $Q=0.41$, and $\Delta\approx1$.

The packing fractions at which we see attenuation peaks are $>20\%$, so it is possible we are observing some aspect of this complicated mode behavior, and not localization. In this interpretation the delayed pulse would then correspond to the "slow" mode, or would be a result of mixing between different modes. This, however, would suggest that the angular frequencies of the delayed pulses should be different from that of the directly transmitted pulse. To within the sensitivity of our detector (sensitive to the resonant frequency $\pm30\%$) we observe no such difference. Also, in their theoretical analysis Sheng *et al.*[32] point out the strong dependence of the slow mode on Q, the ratio of the shear to longitudinal velocities in the solid. When they decrease the ratio Q from 0.41 to 0.19 the "slow" mode all but disappears, even at high packing fractions ($\gtrsim 38\%$). In our experiment Q is low, certainly <0.25, yet we still observe strong resonant absorption peaks for packing fractions below 30%. It is therefore not obvious that our results can be explained solely in terms of an additional propagating mode. Ideally this could be checked by measuring the dispersion relation. Unfortunately our solidifying polymer system does not easily lend itself to Brillouin scattering experiments, so that the measurement is not feasible at present.

In conclusion, we have presented experimental results on acoustic propagation in a solidifying polymer melt. These data indicate that localization can take place in this system, at appropriate excitation frequencies and for appropriate radii of the scattering sites. Transitions between the diffusive and coherent-scattering dominated regimes are evident. We have also observed anomalous forward scattering of a delayed pulse, which we attribute to a coherently reconstructed forward scattered wave. This observation seems to be unique to acoustic experiments such as ours, since the signal we detect must be coherent across the face of the sample. Such measurements would present significant difficulties in optical scattering experiments. We have also noted that previous localization theories do not predict localization in the system we have studied. However, our scattering sites can support shear motion, and we have extended localization theory to take this into account. We find that this leads to strong single-site scattering resonances, which in turn allow for coherent multiple scattering to become important and can lead to fully localized states. We further find that this modified theory predicts localization in our experimental system, once shear excitations are taken into account. However, we note that shear coupling between spheres can significantly complicate the analysis, in particular for high packing fractions and when the shear-wave velocity is large. Such effects are not included in our analysis. Finally, our work suggest that systems composed of solid particles supporting shear suspended in a shear-free fluid may be an extremely useful laboratory for studying acoustic-wave localization in three dimensions.

ACKNOWLEDGMENTS

We wish to thank D. Weitz and L. Ye for stimulating discussions, and for communicating their results prior to publication.

[1]A. Ishimaru, *Wave Propagation and Scattering in Random Media* (Academic, New York, 1978).
[2]A. F. Ioffe and A. R. Regel, Prog. Semicond. **4**, 237 (1960).
[3]P. W. Anderson, Phys. Rev. **109**, 1492 (1958).
[4]P. A. Lee and T. V. Ramakrishnan, Rev. Mod. Phys. **57**, 287 (1985).
[5]G. Bergmann, Phys. Rep. **107**, 1 (1984).
[6]S. John, Phys. Rev. Lett. **53**, 2169 (1984).
[7]E. Akkermans, P. E. Wolf, and R. Maynard, Phys. Rev. Lett. **56**, 1471 (1986).
[8]E. Akkermans, P. E. Wolf, R. Maynard, and G. Maret, J. Phys. (Paris) **49**, 77 (1988).
[9]M. Kaven, M. Rosenbluth, I. Edrei, and I. Freund, Phys. Rev. Lett. **57**, 2049 (1986).
[10]M. Rosenbluth, M. Hoshen, I. Freund, and M. Kaveh, Phys. Rev. Lett. **58**, 2754 (1987).
[11]S. Feng, C. Kane, P. A. Lee, and A. D. Stone, Phys. Rev. Lett. **61**, 834 (1988).
[12]A review of classical-wave localization can be found in *Scattering and Localization of Classical Waves in Random Media*, edited by P. Sheng (World Scientific, Singapore, 1990). See also D. Sornette, Acustica **67**, 575, (1989); *ibid.* **67**, 251 (1979); *ibid.* **68**, 15 (1989).
[13]M. P. van Albada and A. Lagendjik, Phys. Rev. Lett. **55**, 2692 (1985).
[14]S. Etemad, R. Thompson, and M. J. Andrejco, Phys. Rev. Lett. **57**, 575 (1986).
[15]S. Etemad, R. Thompson, M. J. Andrejco, S. John, and F. C. MacKintosh, Phys. Rev. Lett. **59**, 1420 (1987).
[16]I. Edrei and M. Kaveh, Phys. Rev. B **35**, 6461 (1987).
[17]C. H. Hodges and J. Woodhouse, J. Accoust. Soc. Am. **74**, 894 (1983).
[18]S. He and J. D. Maynard, Phys. Rev. Lett. **57**, 3171 (1986).
[19]S. John, H. Sompolinski, and M. J. Stephen, Phys. Rev. B **27**, 5592 (1983).
[20]S. John and M. J. Stephen, Phys. Rev. B **28**, 6358 (1983).
[21]C. M. Soukoulis, E. N. Economou, G. S. Grest, and M. H. Cohen, Phys. Rev. Lett. **62**, 575 (1989).

[22]E. N. Economou and C. M. Soukoulis, Phys. Rev. B **40**, 7977 (1989).
[23]P. Sheng and Z.-Q. Zhang, Phys. Rev. Lett. **57**, 1879 (1986).
[24]C. A. Condat and T. R. Kirkpatrick, Phys. Rev. B **36**, 6782 (1987).
[25]C. A. Condat, J. Accoust. Soc. Am. **83**, 441 (1988).
[26]T. R. Kirkpatrick, Phys. Rev. B **31**, 5746 (1985).
[27]Some of these results have been published in I. S. Graham, L. Piché, and M. Grant, Phys. Rev. Lett. **64**, 3135 (1990).
[28]L. Piché (unpublished).
[29]D. Sornette, Acustica **67**, 199 (1989).
[30]R. Truell, C. Elbaum, and B. B. Chick, *Ultrasonic Methods in Solid State Physics* (Academic, New York, 1969).
[31]D. A. Weitz, J. Liu, L. Ye, and P. Sheng, Phys. Rev. Lett. **65**, 2602 (1990).
[32]P. Sheng, X. Jing, and M. Zhou (unpublished).